maximum load required to break the material was determined. The bone specimens were kept wet in saline during all stages of tissue preparation. After the mechanical test, they were fixed in 10% formalin, decalcified, embedded in paraffin, cut into 4-μm sections and stained with hematoxylin and eosin (H–E).

RNA extraction and reverse transcription polymerase chain reactions (RT-PCR)

Total RNA was extracted from cells using ISOGEN reagent (Nippon Gene, Tokyo, Japan). The cDNA was synthesized using the SuperScript First-Strand Synthesis System (Invitrogen, Carlsbad, CA, USA) and was then incubated with 1 unit of *Escherichia coli* RNase H at 37°C. PCR was performed using Ready to Go PCR beads (Amersham Biosciences, Piscataway, NJ, USA). The oligonucleotide PCR primer sequences and amplification profiles used are described elsewhere [19]. The amplification reaction products were resolved on 2.0% agarose/Tris–acetate buffer gels, electrophoresed at 100 mV and visualized by ethidium-bromide staining. Real-time PCR was preformed to clarify the expression of type X collagen in growth plates of wild-type mice and ob/ob mice. The growth plates of femora and humeri of 4-week-old wild-type mice (n = 4) and ob/ob (n = 4) mice were isolated after aseptic dissection and pounded in liquid nitrogen. Total RNA was extracted from tissue and the cDNA was synthesized, as described above. Real-time PCR was performed using a LightCycler rapid thermal cycler system (Roche Diagnostics) according to the manufacturer's instructions. Reactions were performed in a 20-μl volume with 0.5 μM primers and 2.5 μM $MgCl_2$. Nucleotides, Taq DNA polymerase and buffers were included in the Light-Cycler-DNA Master SYBER Green I Mix (Roche Diagnostics). The plasmid used as the standard DNA was constructed by ligation of a type X collagen PCR product and a G3PDH fragment in pGEM-T Easy vector according to the instructions of the manufacturer (Promega). The concentrations of plasmid preparations were determined by measuring the optical density at 260 nm. The relative amount of gene transcript present was calculated and normalized by dividing the value calculated for the gene of interest by the value calculated for the housekeeping gene. These experiments were repeated three times.

Electron microscopy

Tibiae of 4-week-old wild-type (n = 4) and ob/ob mice (n = 4) were fixed in 2.5% glutaraldehyde and then in OsO_4. The specimens were dehydrated in a graded series of ethanol, embedded in epoxy resin, cut into ultrathin sections and stained with uranium acetate and lead citrate. Sections were examined using a transmission electron microscope (H-300, Hitachi, Tokyo, Japan) operated at 75 kV, and the diameter of collagen fibrils was measured.

TUNEL reaction

Terminal deoxynucleotidyl transferase-mediated dUTP nick end labeling (TUNEL) staining was performed using in situ apoptosis detection kits (TAKARA Bio, Otsu, Japan). Sections cut from paraffin-embedded specimens of the tibiae of 4-week-old (wild type: n = 5, ob/ob: n = 4) and 8-week-old mice (wild type: n = 8, ob/ob: n = 4) were deparaffinized and digested for 15 min with proteinase K (20 μg/ml) at room temperature. The sections were then treated with 3% H_2O_2 in PBS for 20 min to inactivate endogenous peroxidase. The TdT reaction was performed at 37°C for 90 min. Biotinylated nucleotides were detected using streptavidin–horseradish peroxidase conjugate. Diaminobenzidine staining was performed for 10 min at room temperature, resulting in an insoluble colored substrate at the site of DNA fragmentation. The treated sections were counterstained with methyl green. For quantitative evaluation of the number of TUNEL-positive chondrocytes in the hypertrophic zone, the number of positive cells in the hypertrophic zone was counted and expressed relative to the total number of cells in the hypertrophic zone.

Von Kossa staining

Tibiae and femora of 4-week-old mice (wild type: n = 10, ob/ob: n = 6) and 8-week-old mice (wild type: n = 5, ob/ob: n = 4) were fixed in 10% formalin, embedded in glycol methacrylate and cut into 4-μm sections. Von Kossa staining was performed to visualize the matrix mineralization, and toluidine blue staining was performed to visualize the morphology of chondrocytes. Each image, which contained a scale, was photographed and transferred to a computer. The lengths of the growth plate, resting zone, proliferative zone, non-calcified hypertrophic zone and calcified hypertrophic zone were measured using WinROOF software (Mitani-Corp, Fukui, Japan). The zones were defined as follows: the resting zone, lies immediately adjacent to the secondary bony epiphyses; the proliferative zone, occupied by flattened chondrocytes that are aligned in longitudinal columns; and the hypertrophic zone, occupied by spherical and enlarged chondrocytes [20]. The proportional length of each zone to the whole growth plate was calculated. The proportional length of the calcified hypertrophic zone to the whole hypertrophic zone was also calculated.

Treatment of ob/ob mice with leptin

4-week-old ob/ob mice (n = 4) received intraperitoneal injections of either PBS or 50 μg of recombinant murine leptin (Sigma) in a 150-μl volume once a day. 4-week-old wild-type mice (n = 4) also received PBS for 2 weeks. Then, femora, tibiae and humeri were removed, stained with von Kossa and toluidine blue and analyzed for the extent of matrix mineralization, as described above.

Primary culture of nasal septal chondrocytes and mineralization assay

Chondrocytes were isolated from the nasal septal cartilage of a 2-week-old mouse, following a procedure previously described elsewhere [21]. Briefly, after aseptic dissection of the nasal septal cartilage, tissue fragments were incubated for 2 h at 37°C in an enzymatic mixture of 0.25% collagenase type I (Sigma) and 0.1% hyaluronidase type IVS (Sigma). The cells were centrifuged and resuspended in Dulbecco's modified Eagle medium (DMEM) (Gibco BRL, Gaithersburg, MD, USA) containing 5% FBS, 10 mM β-glycerophosphate (Sigma), 50 μg/ml ascorbic acid (Nakarai tesque, Kyoto, Japan), 50 UI/ml of penicillin and 50 μg/ml streptomycin (Gibco BRL). Mineralization in primary culture was determined by staining with alizarin red S. Plates were washed three times with PBS, then stained with 0.5% alizarin red S in H_2O (pH 5.0) for 1 h at room temperature. After staining, plates were washed three times with H_2O and incubated in 100 mM cetylpyridinium chloride for 1 h to solubilize and release calcium-bound alizarin red S into solution [22]. The absorbance of the released alizarin red S was measured at 570 nm. Data are expressed as units of alizarin red S released (1 unit = 1 unit of optical density at 570 nm) per milligram of protein in each culture. The assay was performed in quadruplicate.

ATDC5 cell culture

The ATDC5 mouse chondrocytic cell line, derived from embryonic carcinoma, was used to assess the in vitro effect of leptin on chondrocytic differentiation. Chondrocytic differentiation culture was performed as described in detail elsewhere [23–25]. Briefly, for the first 3 weeks, cells were cultured in a 1:1 mixture of DMEM/F12 medium containing 5% FBS (Gibco BRL), 10 μg/ml human transferrin (Sigma), 3×10^{-8} M sodium selenite (Sigma) and 10 μg/ml bovine insulin (Sigma) at 37°C in a humidified 5% CO_2/95% air atmosphere. Then, the cells were incubated in α-MEM (Gibco BRL) containing 5% FBS, 10 μg/ml human transferrin, 3×10^{-8} M sodium selenite and 10 μg/ml bovine insulin at 37°C in a humidified 3% CO_2/95% air atmosphere. Cells were cultured for a total of 42 days, with medium replacement every 2 days. In some cultures, recombinant mouse leptin (Sigma) was added at final concentrations of 1 pg/ml to 100 μg/ml. The assay was performed in triplicate.

Northern blotting

Total RNA (20 μg) was subjected to electrophoresis on a 1% agarose gel containing 2.2 M formaldehyde. Then, the RNA was transferred to a nylon membrane using a standard method. The probe was a 0.9-kb fragment of mouse α1(X) collagen cDNA labeled with ^{32}P using the Prime It in vitro transcription kit (Stratagene, La Jolla, CA, USA). Hybridization was performed overnight at 65°C. After hybridization, the membranes were sequentially washed at 45°C: twice with 6× saline sodium citrate (SSC) plus 0.5% sodium dodecyl sulphate (SDS), twice with 2× SSC containing 0.1% SDS and twice with 0.2× SSC containing 0.1% SDS. Hybridization signals were detected with a BAS 2500 BioImage analyzer (Fuji Photo Film, Tokyo, Japan). The Northern blot assay was performed two times.

Flow cytometric analysis of apoptosis and the cell cycle

A flow cytometry apoptosis detection kit (Becton Dickinson, Franklin Lakes, NJ, USA) was used to identify programmed cell death. Cells (1×10^5) were suspended in 100 μl of annexin V binding buffer and were then stained with 10 μl fluorescein isothiocyanate-labeled annexin V (to detect phosphatidylserine expression on cells during early apoptotic phases) and 7-aminoactinomycin (7-AAD) (to exclude dead cells) for 15 min at room temperature in the dark. Then, 400 μl of annexin V binding buffer was added, and at least 10,000 cells were analyzed in a FACScan flow cytometer using CellQuest 3.0.1 software (Becton Dickinson). Percentages of cells undergoing apoptosis were determined by dual-color analysis. We repeated the assay four times. The effect of leptin on the cell cycle of ATDC5 cells was investigated by flow cytometric analysis of cells stained with propidium iodide. Briefly, cells were trypsinized, washed in PBS and fixed in 70% ethanol overnight at 4°C until used. Fixed cells were incubated with 1 mg/ml RNase (Sigma) for 60 min at 37°C. Then, 0.25 mg/ml PI (Sigma) was added for 15 min at 4°C in the dark. We acquired 20,000 cells using FACScalliber (Becton Dick-

Table 1
Femoral, humeral lengths and histomorphometric comparisons of proximal tibial growth plates between wild-type and ob/ob mice

	Wild type (n = 10)	ob/ob (n = 6)	P value[a]
Femoral length (mm)	13.9 ± 0.3	12.3 ± 0.3	0.0046
Humeral length (mm)	12.0 ± 0.1	11.5 ± 0.2	0.0105
Resting zone (%)[b]	9.9 ± 1.9	8.3 ± 1.8	0.2002
Proliferation zone (%)[b]	53.6 ± 3.5	49.1 ± 1.8	0.1495
Non-calcified hypertrophic zone (%)[b]	21.0 ± 3.5	4.4 ± 1.8	0.0039
Calcified hypertrophic zone (%)[b]	15.5 ± 6.0	38.1 ± 0.4	0.0039
Proportional length of calcified zone (%)[c]	43.6 ± 9.4	89.7 ± 9.6	0.0001

Summary of the data from two different experiments was shown.
[a] Statistical differences were analyzed by Mann–Whitney U test.
[b] Proportional length of resting, proliferation, non-calcified hypertrophic or calcified hypertrophic zone (%) represents the ratio of the length of growth plate in tibia.
[c] Proportional length of calcified zone (%) represents the ratio of the length of calcified hypertrophic zone to that of whole hypertrophic zone.

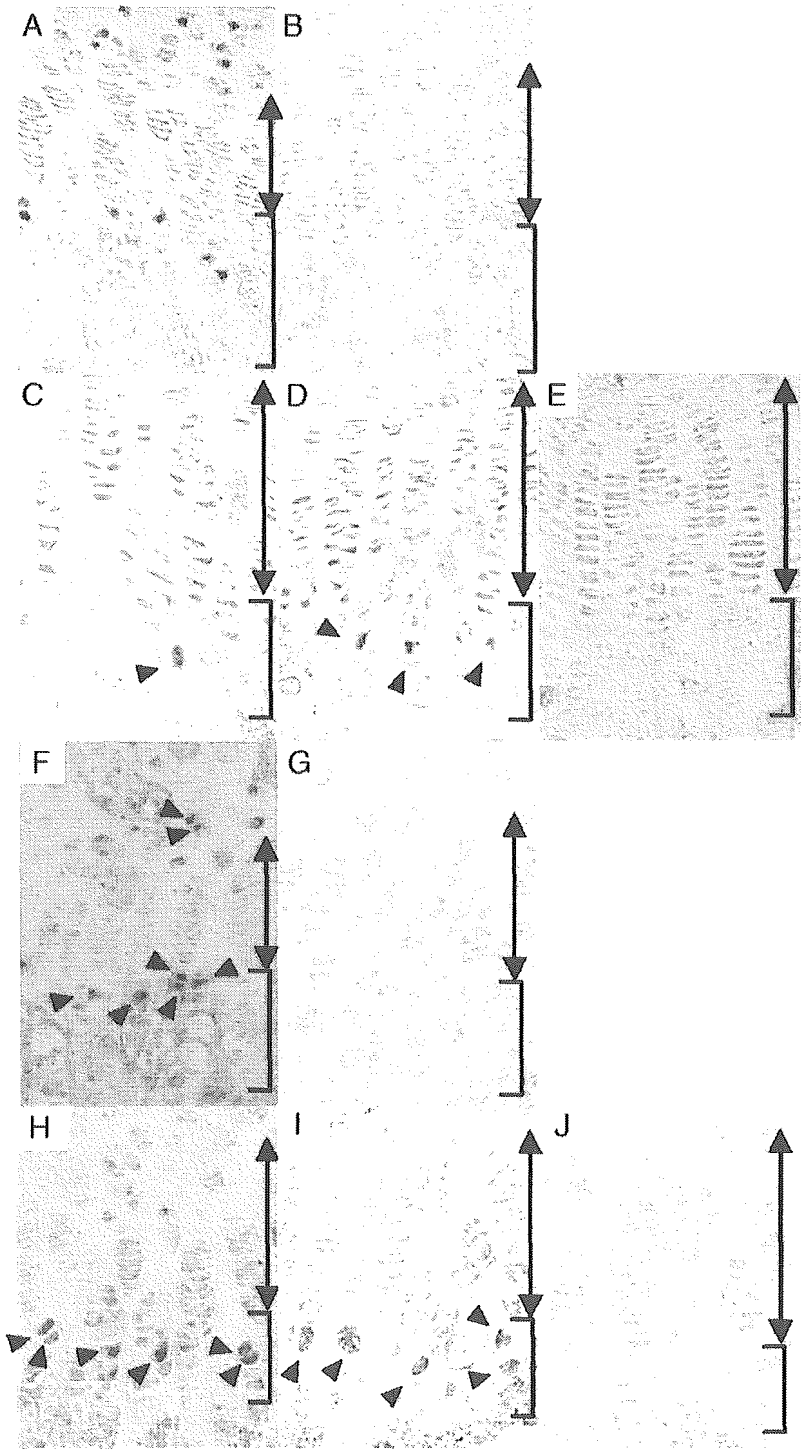

Fig. 1. Immunohistochemical localization of leptin (A, B) and leptin receptor (C, D, E) in the growth plates of 4-week-old wild-type mice (A, C, E) and ob/ob mice (B, D). Leptin expression was identified in resting and prehypertrophic chondrocytes in wild-type mice (A). Ob-Rb was identified in terminal hypertrophic chondrocytes in wild-type (C) and ob/ob (D) mice (arrowheads). (E) Negative controls without primary antibodies. Brackets indicate hypertrophic zones and bidirectional arrows indicate proliferative zones. In situ hybridization of leptin (F, G) and leptin receptor (H, I, J) in the growth plates of 4-week-old wild-type mice (F, H, J) and ob/ob mice (G, I). Expression of leptin mRNA was identified in resting and prehypertrophic chondrocytes in wild-type mice (F) (arrowheads). Ob-Rb mRNA was identified in terminal hypertrophic chondrocytes in wild-type (H) and ob/ob (I) mice (arrowheads). (J) Sense probe. Brackets indicate hypertrophic zones and bidirectional arrows indicate proliferative zones. Magnification: ×400.

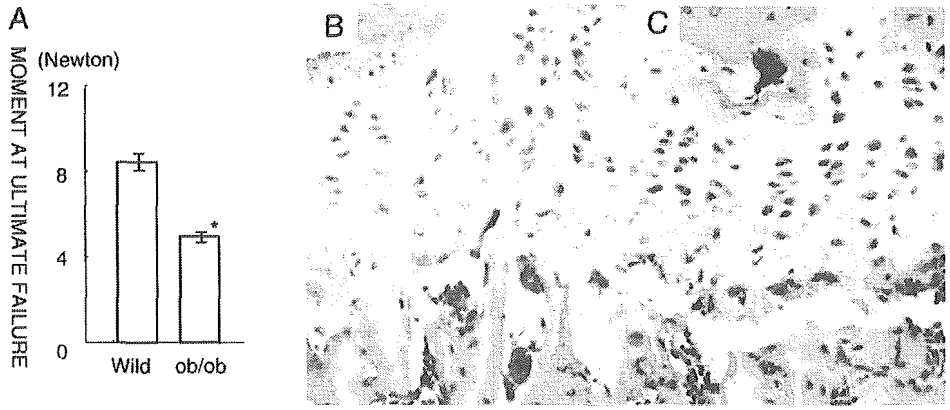

Fig. 2. Mechanical properties of the growth plates. (A) Maximum load required to break the growth plates of 8-week-old wild-type (n = 10) and ob/ob (n = 6) mice. Values are the mean ± SD of the data from two different experiments. Growth plates of ob/ob mice were significantly more fragile than those of wild-type mice (*P = 0.001). (B, C) Histological microphotograph showing that the proximal tibial growth plates of wild-type mouse (B) and ob/ob mouse (C) broke at the chondro-osseous junction. H–E staining. Magnification: ×400.

inson). Data were analyzed using ModFitLT 3.0 software (Becton Dickinson). These experiments were repeated three times. The proliferation index, which is the number of cells in both S and G_2M divided by the total cell number, was calculated.

Measurement of calcium content

Calcium content was measured by the OCPC (ortho-cresolphthalein complexone) method using a calcium C-test Wako kit (Wako Pure Chemical, Tokyo, Japan). First, 200 μl of 2 N hydrochloric acid was added to the wells, followed by shaking at room temperature overnight. Samples were then frozen at −20°C until used. At the time of measurement, 50 μl of sample was added to 5 ml of buffer and 500 μl of substrate. The calcium solution provided in the kit was used to generate a standard curve. The plate was incubated at room temperature for 5 min and then read at 570 nm. We repeated the assay four times.

Statistical analysis

Data are presented as mean ± standard deviation. Groups were compared by analysis of variance (ANOVA) followed by analysis with Fisher's PLSD for multiple comparisons. Individual groups were compared using the Mann–Whitney U test for unpaired analysis. Differences between treatment groups were considered significant at $P < 0.05$.

Results

Ob/ob mice have shorter femora and humeri than wild-type mice

The femora and humeri of 4-week-old wild-type mice and ob/ob mice were measured. The femoral and humeral lengths of ob/ob mice were significantly shorter than those of wild-type mice (Table 1).

Prehypertrophic chondrocytes express leptin and terminal hypertrophic chondrocytes express leptin receptor

The expression of leptin and its receptor in the femora, tibiae and humeri from 4-week-old wild-type mice was examined by immunohistochemistry and in situ hybridization. Leptin mRNA and protein expression was observed in resting and prehypertrophic chondrocytes in the growth plates of wild-type mice (Figs. 1A and F). No leptin expression was detected in the proliferative or hypertrophic zone. Positive staining for leptin receptor mRNA and protein was observed in terminal hypertrophic chondrocytes in both wild-type and ob/ob mice (Figs. 1C, D, H and I).

Fig. 3. Histological and histochemical analyses of 4-week-old wild-type mice and ob/ob mice. (A–D) Von Kossa and toluidine blue double staining of tibiae of wild-type mice (A, C) and ob/ob mice (B, D). In wild-type mice, the proportional length of calcified hypertrophic zone to whole hypertrophic zone was less than 50%. However, in ob/ob mice, most part of hypertrophic zone was mineralized. The column structure of proliferating and hypertrophic chondrocytes was also disturbed. Brackets indicate the entire hypertrophic zone, and bidirectional arrows indicate the calcified hypertrophic zone. Magnifications: ×100 (A, B) and ×400 (C, D). (E, F) The expression level of type X collagen in the growth plates of femora and humeri of 4-week-old wild-type mice (n = 4) and ob/ob (n = 4) mice. The amplified PCR products were 459 base pair (bp) for type X collagen and 307 bp for G3PDH (E). Real-time PCR analyses of expression level of type X collagen in the femoral and humeral growth plates of wild-type mice and ob/ob mice (F). Values are given as mean ± SD. Type X collagen expression in growth plates of ob/ob mice was significantly less than that of wild-type mice (*P = 0.0357). (G, H) Electron microscopy images of the hypertrophic zone of wild-type mice (G) and ob/ob mice (H). In wild-type mice, collagen fibrils ran parallel to one another, whereas in ob/ob mice, collagen fibrils showed less-organized loose reticular arrangement. Magnification: ×30,000. (I, J) TUNEL staining of the hypertrophic zone of wild-type mice (I) and ob/ob mice (J). The percentage of hypertrophic chondrocytes that were TUNEL positive was greater in ob/ob mice than in wild-type mice.

Ob/ob mice have fragile growth plates

The growth plates of ob/ob mice were significantly more fragile than those of wild-type mice (Mann–Whitney U test, $P = 0.001$). The average force at ultimate failure was 8.4 ± 1.5 N for wild-type segments and 4.9 ± 0.6 N for ob/ob segments (Fig. 2A). After the mechanical test, all samples were processed for histological examination. The breakage occurred at the chondro-osseous junction in all tibiae regardless of the genotype (Figs. 2B and C).

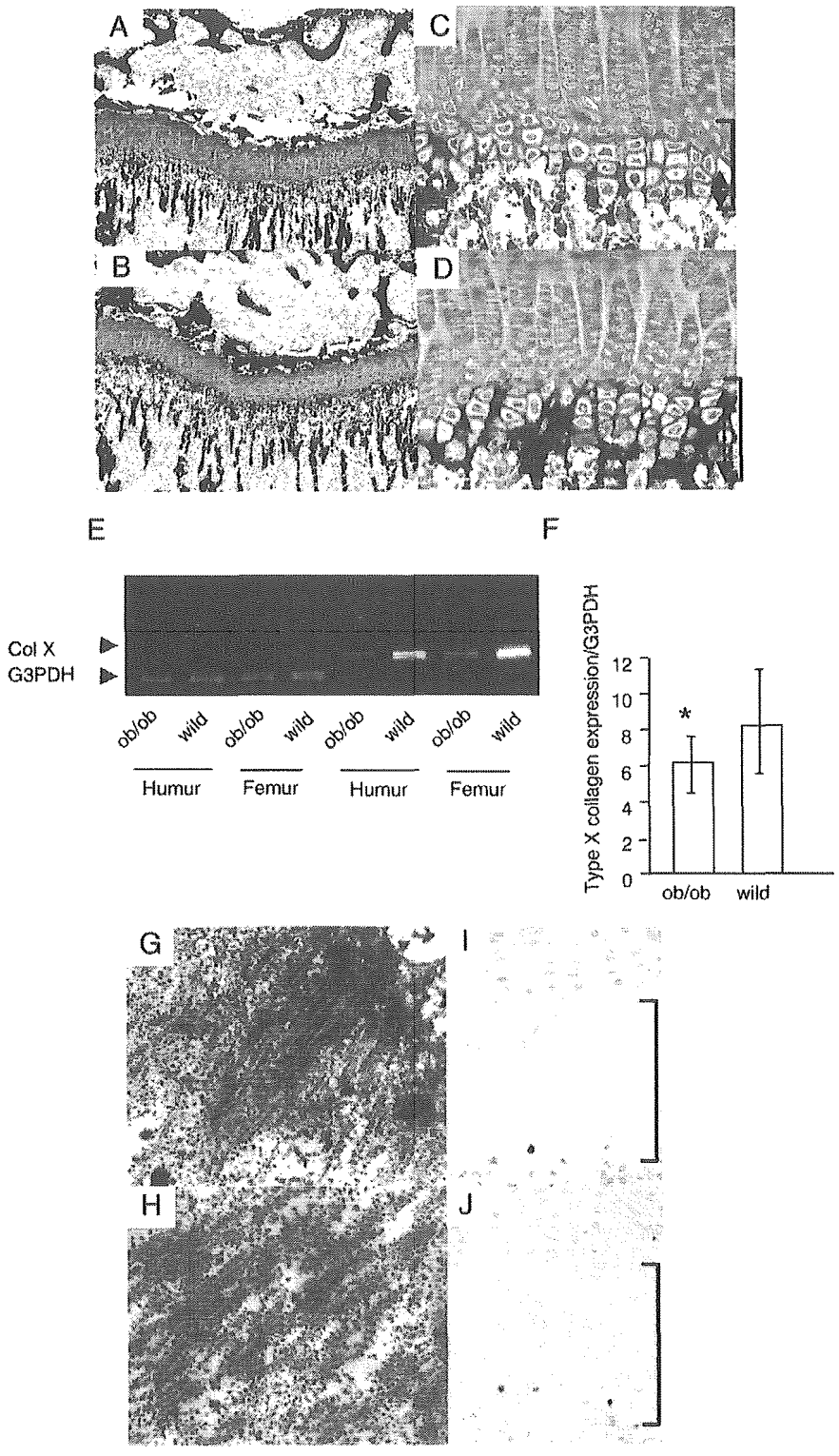

Alterations in morphology, mineralization, type X collagen expression, matrix microstructure and chondrocyte apoptosis in the growth plates of ob/ob mice

Higher magnification of eosin-stained and von Kossa-stained sections revealed that the column structure of proliferating and hypertrophic chondrocytes was disturbed. The majority of the columns in ob/ob mice seemed to be bent or twisted, and the chondrocytes were poorly aligned. In some columns, chondrocytes were distributed like pebble stones rather than a column. Matrix mineralization was also altered in 4-week-old ob/ob mice. In wild-type mice, the proportional length of the calcified hypertrophic zone to the whole hypertrophic zone was less than 50% (Figs. 3A and C; Table 1). However, in ob/ob mice, most of the hypertrophic zone was mineralized (Figs. 3B and D; Table 1). The proportional length of the calcified hypertrophic zone to the whole hypertrophic zone in the ob/ob mice was significantly greater than that of wild-type mice (Table 1, Mann–Whitney U test, $P = 0.0001$), whereas there was no detectable difference in the proportional length of the other zones to the growth plate.

In situ hybridization assays found no difference in mRNA expression of type II or type X collagen in wild-type and ob/ob mice (data not shown). However, the expression level of type X collagen in the growth plates of ob/ob mice was lower than that in wild-type mice (Fig. 3E). Real-time PCR showed that the expression level of type X collagen in ob/ob mice was 0.48-fold the expression level in wild-type mice (ob/ob mice: 4.4 ± 2.7; wild-type mice: 9.2 ± 7.4%; Mann–Whitney U test, $P = 0.0357$) (Fig. 3F).

We examined the collagen fibril microstructure in the hypertrophic zone by transmission electron microscopy. There was no significant difference in the diameter of collagen fibrils from 4-week-old wild-type mice and ob/ob mice (data not shown). However, electron microscopy of the hypertrophic zone of 4-week-old ob/ob mice revealed a less-organized loose reticular distribution of collagen fibrils (Fig. 3H), in contrast to the well-organized parallel collagen fibrils in wild-type mice (Fig. 3G).

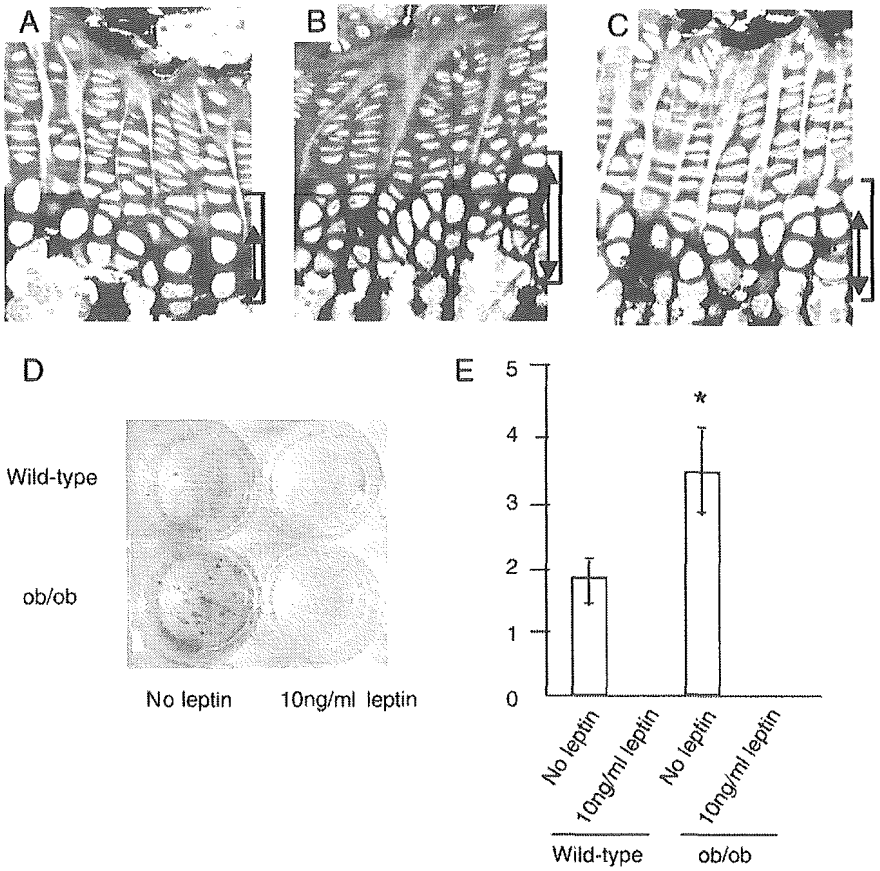

Fig. 4. Cartilage matrix mineralization in ob/ob mouse and the effect of leptin treatment. (A, B, C) Von Kossa/toluidine blue double staining of tibial growth plates of wild-type mice treated with PBS (A), ob/ob mice with PBS (B) and ob/ob mice with leptin (C) for 2 weeks. Brackets indicate whole hypertrophic zones and bidirectional arrows indicate calcified hypertrophic zones. Magnification: ×400. (D, E) Mineralization in primary culture of nasal septal chondrocytes of wild-type mice and ob/ob mice. Mineral deposit was stained by alizarin red S (D) and quantified the absorbance of the solubilized alizarin red S at 570 nm (E) as described in Material and methods. The assay was performed in quadruplicate. Values are given as mean ± SD. On days 17, mineralization occurred in the both types of cells without leptin, whereas no mineralization was found in cultures with leptin (D). A quantitative analysis revealed that matrix mineralization in cultures of ob/ob chondrocytes without leptin was significantly more than others than others (ANOVA, $*P < 0.0001$).

During the terminal differentiation process, growth plate chondrocytes undergo apoptosis with degradation and calcification of cartilaginous matrix followed by deposition of bone matrix. The number of TUNEL-positive chondrocytes in the hypertrophic zone was quantified as a percentage of the total number of cells in the hypertrophic zone. In 4-week-old wild-type mice, the percentage of apoptotic TUNEL-positive cells among hypertrophic chondrocytes was 10.6 ± 0.6% (Fig. 3I). However, in 4-week-old ob/ob mice, the number of apoptotic chondrocytes in the hypertrophic zone (Fig. 3J) was significantly greater (14.7 ± 1.8%, Mann–Whitney U test, $P = 0.02$). In 8-week-old mice, no alterations in growth plate cartilage were detected (data not shown).

Leptin administration increased bone length and altered matrix mineralization in growth plate cartilage in ob/ob mice

To investigate whether peripheral administration of leptin could rescue the various phenotypes in the growth plate of ob/ob mice, we performed rescue experiments using recombinant mouse leptin. Treatment of 4-week-old ob/ob mice with leptin for 2 weeks significantly increased humeral length by 3.8% ($P < 0.0001$) and femoral length by 4.9% ($P = 0.0001$) as compared to PBS-treated ob/ob mice. However, leptin treatments did not restore the decreased long bone length in ob/ob mice to the level of that in wild-type mice. Double staining of tibiae with von Kossa and toluidine blue was performed to examine matrix mineralization. The proportional length of the calcified hypertrophic zone to the whole hypertrophic zone in the ob/ob mice treated with leptin was significantly shorter than in PBS-treated ob/ob mice; however, it showed no statistical difference when compared with wild-type mice (Figs. 4A–C; Table 2). These data indicate that leptin treatment for 2 weeks completely rescued the increased mineralization of the hypertrophic zone in growth plates of ob/ob mice.

Table 2
Effect of leptin treatment on long bone length and histomorphometric parameters in proximal tibial growth plate of ob/ob mouse

	Wild ($n = 4$)	ob/ob ($n = 4$)	ob/ob treated with leptin ($n = 4$)
Femoral length (mm)	14.9 ± 0.1	13.5 ± 0.1[a]	14.2 ± 0.1[a]
Humeral length (mm)	13.5 ± 0.1	12.4 ± 0.1[a]	12.9 ± 0.1[a]
Resting zone (%)[b]	11.8 ± 1.1	11.0 ± 1.0	9.9 ± 0.7
Proliferation zone (%)[b]	46.5 ± 1.8	42.2 ± 1.1	40.6 ± 2.2
Non-calcified hypertrophic	19.0 ± 1.3	17.8 ± 2.5[a]	23.3 ± 2.3[a]
Calcified hypertrophic zone (%)[b]	22.9 ± 1.5	29.1 ± 0.7[a]	23.9 ± 1.9
Proportional length of calcified zone (%)[c]	54.7 ± 1.1	62.2 ± 3.6[a]	51.1 ± 4.2

[a] Statistical differences from wild-type mice were analyzed by one factor ANOVA followed by analysis with the Fisher's PLSD for multiple comparisons.

[b] Proportional length of resting, proliferation, non-calcified hypertrophic or calcified hypertrophic zone (%) represents the ratio of the length of growth plate in tibia.

[c] Proportional length of calcified zone (%) represents the ratio of the length of calcified hypertrophic zone to that of whole hypertrophic zone.

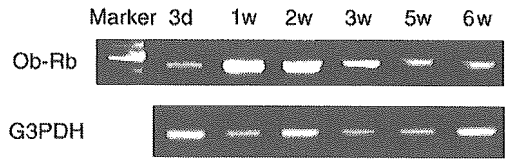

Fig. 5. RT-PCR analysis of leptin receptor expression in ATDC5 chondrocytic cells. Top: mRNA expression of the long-form variant of the leptin receptor Ob-Rb was detected in ATDC5 cells throughout the chondrocytic differentiation culture period. Bottom: G3PDH mRNA expression was used as a control.

Increased matrix mineralization in primary culture of chondrocytes from ob/ob mice

To assess the autocrine/paracrine effect of endogenous leptin on chondrocyte differentiation, we isolated and then cultured chondrocytes from the nasal septal cartilage of 14-day-old wild-type mice and ob/ob mice. Twenty-four hours after seeding, cells were incubated with or without 10 ng/ml of leptin. The cells from both ob/ob and wild-type mice exhibited polygonal shapes on day 5, and cells cultured in the absence of exogenous leptin changed to round shapes. The morphological changes were limited in the cells from wild-type and ob/ob mice incubated with leptin. On day 17, alizarin red S staining revealed that mineralization had occurred in both types of cells without leptin, whereas no mineralization was found in cultures with leptin (Fig. 4D). A quantitative analysis revealed that matrix mineralization in cultures of ob/ob chondrocytes without leptin was significantly greater than in the other cell cultures (ANOVA, $P < 0.0001$) (Fig. 4E).

ATDC5 cells express leptin receptor

To study the mechanisms of the effects of leptin on the growth plate, we evaluated the effects of leptin on ATDC5 cells. These cells differentiate into chondrocytes, serially

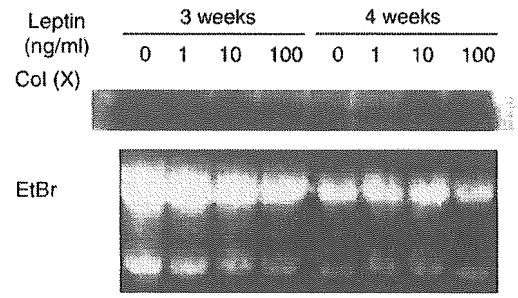

Fig. 6. Northern blot analysis of type X collagen mRNA in ATDC5 cells. ATDC5 cells were cultured with or without leptin at a concentration of 1 ng/ml, 10 ng/ml or 100 ng/ml for 3 weeks or 4 weeks. The bottom panels show the ethidium bromide-stained gels.

express several differentiation markers for chondrocytes and mineralize [23–25]. Therefore, ATDC5 cells provide an excellent model for the study of the molecular mechanisms underlying the regulation of cartilage differentiation during endochondral ossification.

A previous report showed that MCC-5, a mouse chondrocyte cell line, secreted leptin [9]. Therefore, as a preliminary experiment, leptin released by ATDC5 cells into the culture medium was measured in the supernatants in duplicate using a mouse leptin ELISA system (TECHNE, Minneapolis, MN, USA). The limit of sensitivity for leptin was 22 pg/ml. Leptin protein was not detected in the culture media at any of the testing time points (3 days, and 1, 2, 3, 4, 5 and 6 weeks; data not shown). The long-form variant of the leptin receptor (Ob-Rb), which is the most functional isoform of the leptin receptor, was detected in ATDC5 cells at all testing time points in the culture period (Fig. 5).

Leptin altered the type X collagen expression pattern in ATDC5 cell culture

We next used Northern blots to examine the effect of exogenous leptin on mRNA expression of type X collagen, which is a marker for hypertrophic chondrocytes, in ATDC5 cell differentiation (Fig. 6). It was reported that type X collagen mRNA was not expressed at the beginning of ATDC5 cell differentiation in culture and that the expression was greatest at 3–4 weeks of culture [25]. In our experiments, when cells were cultured without leptin, abundant type X collagen mRNA expression was detected at 3 weeks, but this signal markedly decreased at 4 weeks. When cells were cultured in the presence of 1 or 10 ng/ml of leptin, which is equivalent to the normal serum concentration of leptin [26,27], type X collagen mRNA was steadily expressed both at 3 and 4 weeks. In the presence of 100 ng/ml leptin, type X collagen expression was profoundly low at 3 weeks; however, delayed and less abundant upregulation was observed at 4 weeks.

Leptin inhibited apoptosis and cell growth in ATDC5 cell culture

In two-color FACS analysis of apoptosis in ATDC5 cell culture, no apoptotic cells (annexin V positive/7-AAD negative) were detected at 3 weeks. At 4 weeks, many apoptotic cells were detected among cells cultured without leptin, whereas few apoptotic cells were detected among cells cultured in the presence of leptin (Figs. 7A–F). At 5 and 6 weeks, although the proportion of apoptotic cells to total cells increased with time in the presence or absence of leptin, the cells cultured in the presence of leptin exhibited a lower degree of apoptosis than those cultured without leptin at every time point tested (Figs. 7G–I). Throughout the culture period, physiological doses of leptin (1 and 10 ng/ml) steadily inhibited cell apoptosis. However, a dose of leptin lower than the normal serum level showed weak suppression of chondrocyte apoptosis especially at 4 and 5 weeks, and higher doses of leptin (>100 ng/ml) at 6 weeks showed weak suppression. The dose–response curve of leptin inhibition of ATDC5 cell apoptosis seemed to be bell shaped. We performed a study of leptin's effects on the cell cycle of chondrocytes using FACS analysis. There was no significant difference in the proliferation index between ATDC5 cells treated with or without leptin until 3 weeks (data not shown). However, as shown in Fig. 7 and Table 3, exogenous leptin treatment resulted in a reduced growth fraction starting from 4 weeks, and the proliferation index of ATDC 5 cell culture with leptin at every concentration was significantly lower than that without leptin at 5 and 6 weeks. Taken together, our results indicate that leptin suppressed apoptosis and proliferation of ATDC5 cells.

Leptin inhibited matrix mineralization in ATDC5 cell culture

Starting after 5 weeks of culture, calcification of the matrix was detectable in ATDC5 cells. However, in the presence of leptin at every concentration tested (1 pg/ml–100 μg/ml), matrix calcification was inhibited at 5 and 6 weeks. Interestingly, a physiological concentration of leptin (1–10 ng/ml) abolished the production of calcified matrix by ATDC5 cells (Fig. 8). The dose–response curve of leptin inhibition of ATDC5 matrix mineralization seemed to be bell shaped.

Discussion

In addition to hypothalamic regulation of metabolic rate and food intake, leptin is reportedly important for fetal growth [28]. Recently, leptin has been shown to regulate bone formation via the sympathetic nervous system [29,30]. However, some investigators have claimed that leptin also has a direct effect on peripheral tissues via its receptor [6,18,31,32]. Peripheral leptin administration has been shown to restore the reduced femoral length of limbs in ob/ob mice [8]. Some researchers have found that Ob-Rb is expressed in cartilaginous skeletal growth centers, articular

Fig. 7. Flow cytometric quantification of the effect of leptin on apoptosis and the cell cycle in ATDC5 cells. (A–F) Representative data from flow cytometric analyses for apoptosis of ATDC5 cells cultured without leptin (A) or with leptin at a concentration of 1 ng/ml (B), 10 ng/ml (C), 100 ng/ml (D), 1 μg/ml (E) or 100 μg/ml (F) for 4 weeks. Dots in the right bottom corner (boxed area) of each graph represent apoptotic cells. (G–I) The ratio of the apoptotic cell number to the total cell number at 4 weeks (G), 5 weeks (H) and 6 weeks (I). Representative data from four repeated experiments are shown. Values are mean ± SD. *Values significantly different from those of cells cultured without leptin (ANOVA). (J–O) Representative cell cycle data from flow cytometric analyses of ATDC5 cells cultured without leptin (J) or with leptin at a concentration of 1 ng/ml (K), 10 ng/ml (L), 100 ng/ml (M), 1 μg/ml (N) or 100 μg/ml (O) for 4 weeks. These experiments were repeated three times.

cartilage and osteoblasts [6,31–33]. In the present study, we analyzed long bones of ob/ob mice, focusing on the growth plates. We confirmed that leptin is expressed in resting and prehypertrophic chondrocytes in growth plate and that its receptor is expressed in terminal hypertrophic chondrocytes, that the femoral and humeral lengths of ob/ob mice were shorter than those of wild-type mice and that treatment with recombinant leptin rescued the reduced femoral and humeral

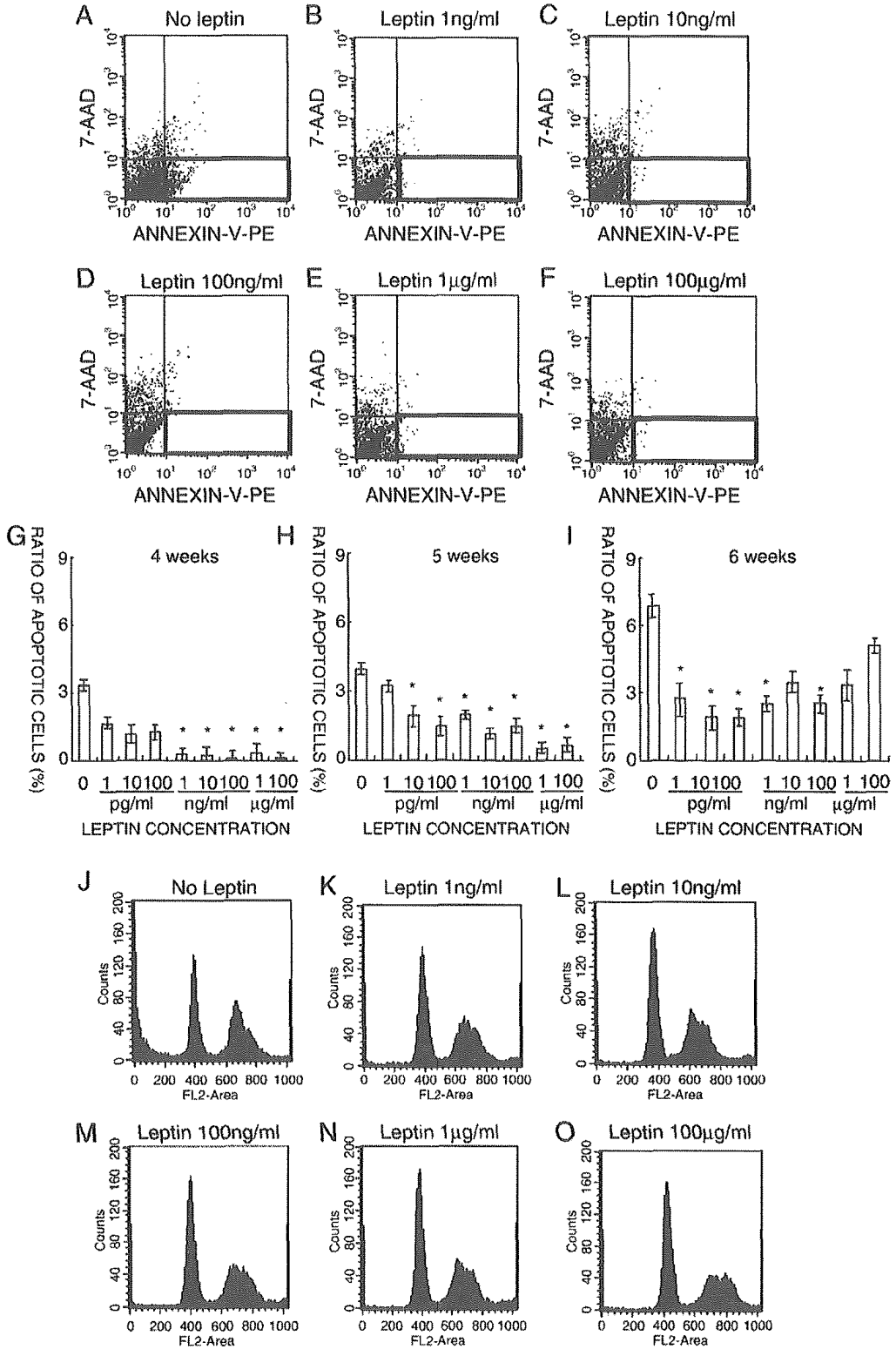

Table 3
Effect of leptin on cell cycle by flow cytometry

	G0/G1[a]	PI[b]
No leptin (4 weeks)	40.9 ± 1.0	55.52 ± 0.600
Leptin 1 ng/ml (4 weeks)	47.9 ± 3.4[c]	52.153 ± 3.143
Leptin 10 ng/ml (4 weeks)	50.5 ± 1.3[c]	49.527 ± 1.299
Leptin 100 ng/ml (4 weeks)	49.2 ± 1.9[c]	50.763 ± 1.886
Leptin 1 μg/ml (4 weeks)	51.4 ± 2.6[c]	48.577 ± 2.568[c]
Leptin 100 μg/ml (4 weeks)	51.4 ± 5.9[c]	48.650 ± 5.901[c]
No leptin (5 weeks)	37.6 ± 0.5	58.460 ± 0.836
Leptin 1 ng/ml (5 weeks)	49.3 ± 1.1[c]	48.690 ± 1.199[c]
Leptin 10 ng/ml (5 weeks)	48.7 ± 0.6[c]	50.170 ± 0.1411[c]
Leptin 100 ng/ml (5 weeks)	49.3 ± 1.0[c]	49.233 ± 0.569[c]
Leptin 1 μg/ml (5 weeks)	50.7 ± 0.5[c]	48.777 ± 0.479[c]
Leptin 100 μg/ml (5 weeks)	57.6 ± 1.1[c]	41.750 ± 1.262[c]
No leptin (6 weeks)	31.8 ± 0.8	61.347 ± 0.660
Leptin 1 ng/ml (6 weeks)	48.8 ± 2.1[c]	48.643 ± 3.393[c]
Leptin 10 ng/ml (6 weeks)	43.2 ± 3.3[c]	53.400 ± 2.858[c]
Leptin 100 ng/ml (6 weeks)	43.6 ± 0.6[c]	53.800 ± 2.755[c]
Leptin 1 μg/ml (6 weeks)	47.0 ± 4.3[c]	48.613 ± 3.393[c]
Leptin 100 μg/ml (6 weeks)	51.2 ± 2.8[c]	43.713 ± 1.954[c]

Values indicate mean ± SD of the data from three independent experiments.
[a] Proportion (%) of cells in G0 and G1 cycle/the total cells.
[b] The proliferation index = (cells of S and G_2M)/the total cells).
[c] Statistical differences from the cell without leptin at the same period were analyzed by one factor ANOVA.

lengths in ob/ob mice. In addition, we showed that cartilaginous matrix of hypertrophic zone of ob/ob mouse showed premature mineralization and that the increased mineralization in ob/ob hypertrophic zone was restored by the treatment with recombinant leptin. Moreover, in the primary cultures of chondrocytes from ob/ob mice, where no endogenous leptin existed, matrix mineralization increased as compared to the cultures of chondrocytes from wild-type mice, suggesting that the endogenous leptin inhibited the matrix mineralization. The addition of exogenous leptin of physiological serum level to those cultures completely abolished the mineralization. Taken together, these findings suggest that leptin functions as a paracrine factor via Ob-Rb during normal chondrocyte differentiation, which is similar to the mechanism that has been proposed for regulation of chondrocyte differentiation in the growth plate by parathyroid hormone related protein (PTHrP).

The hypertrophic zone, in which Ob-Rb is expressed, plays a key role in endochondral ossification. The hypertrophic zone undergoes matrix calcification, capillary invasion and chondrocyte apoptosis, which eventually leads to cartilage matrix degeneration and bone matrix deposition. In the present study, we confirmed that the femoral and humeral lengths of ob/ob mice were shorter than those of wild-type mice. We also found that the growth plates of ob/ob mice were more fragile than those of wild-type mice (as determined by a mechanical test) and were easily broken at the chondro-osseous junction. Although there was no apparent difference in the microscopic appearance of the zonal structure of the growth plate or mRNA expression of type II or X collagen (as determined by in situ hybridization), the local expression level of type X collagen in the growth plate (as determined by real-time PCR) was reduced in ob/ob mice as compared to wild-type mice. Electron microscopy of the hypertrophic zone of ob/ob mice showed a less organized collagen fibril arrangement. The number of apoptotic chondrocytes in the hypertrophic zone was significantly greater in ob/ob mice. The majority of the hypertrophic zone was mineralized in ob/ob mice, and the peripheral administration of leptin in ob/ob mice restored the increased proportional length of the calcified hypertrophic zone to the whole hypertrophic zone down to a level

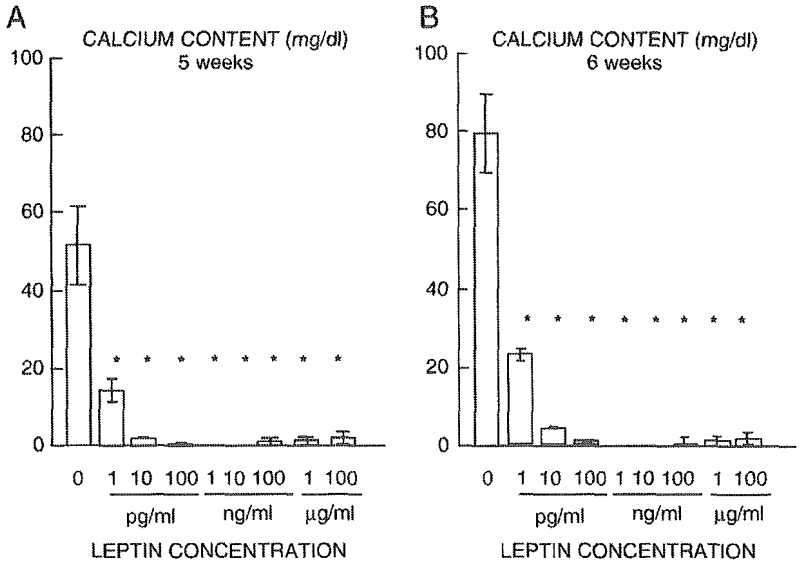

Fig. 8. The effect of exogenous leptin on matrix mineralization of ATDC5 cells incubated for 5 weeks (A) and 6 weeks (B). The calcium content of each culture well was measured using the OCPC method and was expressed as mean ± SD. *Values significantly different from those of cultures without leptin (ANOVA). Representative data from four different experiments were shown.

close to that of wild-type mice. Furthermore, we showed that in primary cultures of chondrocytes from ob/ob mice, where no endogenous or exogenous leptin existed, matrix mineralization was increased as compared to cultures of chondrocytes from wild-type mice without leptin treatment or other cultures in the presence of exogenous leptin. These findings are consistent with those of our in vitro experiments using ATDC5 cells. These experiments clearly indicated that 1–10 ng/ml of leptin, which is equivalent to normal circulating levels, strongly inhibited matrix mineralization, decreased the rate of apoptosis and altered the type X collagen expression pattern, which reportedly plays an important mechanical role in the hypertrophic zone [34,35]. Among the alterations in the growth plates of ob/ob mice that were observed, those associated with matrix maturation such as reduced expression of type X collagen, disturbed collagen arrangement and premature mineralization may be important for the etiology of fragile growth plate.

Montague et al. described a highly obese patient with congenital leptin deficiency who developed a leg deformity requiring corrective limb surgery [10]. Although a precise description explaining the cause of the deformity was not provided, it is unlikely that the obesity alone would cause limb deformity requiring corrective surgery. We hypothesize that growth plate fragility caused by leptin deficiency is associated with the development of metaphysical deformities in patients with congenital leptin deficiency. One of the best-known clinical manifestations of growth plate fragility is slipped capital femoral epiphysis, which is closely associated with obesity [36]. Although there have been no reports describing serum leptin levels in patients with slipped capital femoral epiphysis, it has been reported that the serum leptin level of obese children is approximately five times that of control children [37].

Interestingly, in the present in vitro experiment, the dose–response curve of leptin inhibition of chondrocyte apoptosis and mineralization seemed to be bell shaped, and a dose of leptin higher than the normal serum level, as well as a lower dose, showed weak suppression of chondrocyte apoptosis and mineralization. These findings suggest that the high serum leptin concentration in obese children is involved in the etiology of slipped capital femoral epiphysis.

There have been several reports that leptin may play an important physiological role in skeletogenesis. Ducy et al. reported that leptin inhibits bone formation [29]. However, other researchers showed that leptin stimulates bone formation [6,8,38]. A very recent report showed that leptin also regulates bone resorption through osteoblast function to support osteoclastogenesis in a complicated manner via the sympathetic nerve system and other molecules [39]. There have been conflicting reports of the skeletal phenotype of ob/ob mice [40]. Some studies concluded that ob/ob mice have increased bone mass in dual X-ray absorptiometry analyses and/or histomorphometric analyses of femora, while other studies showed reduced bone mass based on their examinations of femoral and whole body bone mass [8,29,30,40]. With regard to longitudinal bone growth, most of the observations (including the current study) reported that the long bone length is shorter in ob/ob mice than in wild-type mice. Because linear growth occurs by endochondral bone formation at the epiphyseal growth plate, these observations suggest a potential role for leptin in endochondral ossification. Usually, premature mineralization of the growth plate results in impaired longitudinal bone growth [41]. Therefore, our findings that the hypertrophic zone in the growth plates of ob/ob mice showed premature mineralization may explain, at least in part, the shortening of long bones in leptin deficiency. A recent and precise report on skeletal manifestations in ob/ob mice showed that ob/ob mice at 6 months of age had shorter femora, whereas they exhibited longer vertebral body length [40]. In our observations in 4-week-old mice, we observed a trend that the vertebral length of ob/ob mice was longer (Mann–Whitney U test, $P = 0.06$, data not shown), which dose not contradict the previous reports. The reason why we did not find a significant difference in vertebral body length may be attributed to the difference in the age at the time of observation. Authors of the previous study suggested that the effect of leptin signaling on skeletogenesis is affected by weight, activities, gravity and muscle force [40]. Because ob/ob mice start to gain weight and lose muscle mass at 3 or 4 weeks of age, our observations must be under minor influence of such mechanical factors and muscle mass compared to the previous study in which 6-month-old mice were used. In view of these points, these observations suggest that the shortening of bone length is the primary manifestation of leptin deficiency and that the increase in vertebral body length is a secondary phenotype caused by the various abnormalities, including mechanical factors that are associated with leptin deficiency. It is also possible that the vertebral growth plate responds to the absence of leptin signals in a fundamentally different manner than the long bone growth plate.

Ob/ob mice have been noted to show an increased number of bony trabeculae in long bones that are thinner than those of wild-type mice [40]. Since trabeculae in primary spongiosa initially form between columns of hypertrophic chondrocytes, the alteration in hypertrophic zones that we found in ob/ob mice may be implicated in the unique trabecular phenotype. However, we could not find any statistical difference in histomorphometric analyses on columnar structure in hypertrophic zone including column number and calcification column thickness, or trabecular structure in primary spongiosa including trabecula number and thickness (data not shown).

In the present study, we proposed the possible involvement of direct local regulatory mechanisms of leptin in the growth plate, and we demonstrated the altered chondrocyte differentiation and matrix maturation in ob/ob mice. In addition, ob/ob mice have multiple endocrine abnormalities, such as hypercortisolism, hypogonadism and hyperinsulinemia, known to regulate

endochondral ossification [42,43]. Treatment of ob/ob mice with peripherally administered leptin could not completely achieve the femoral length of wild-type mice [3], suggesting that the effect of leptin on bone development is a combined result of a direct local endocrine/paracrine mechanism and an indirect mechanism via the central nervous system. The downstream target of leptin in chondrocytes is unknown. Because leptin modulates a variety of events associated with terminal differentiation, the target seems likely to be an essential regulatory factor in endochondral ossification, such as PTHrP and Indian hedgehog.

Although our findings indicated that the femoral and humeral length of ob/ob mice was short, the alternations in chondrocyte apoptosis and cartilage matrix mineralization were transient and we found no morphological abnormalities in the growth plates of 8-week-old ob/ob mice. Currently, we have no evidence-based explanation for the transient presentation of the morphological phenotypes in ob/ob mice growth plates. To better understand the mechanism, we need additional investigations regarding the age-related alteration of the downstream target of leptin in chondrocytes, other molecules that compensate for leptin's effect, signaling pathways that mediate or interact with leptin signaling as well as the regulation of Ob-Rb expression, all of which may modulate the chondrocyte response to leptin.

In conclusion, we found that the growth plates of ob/ob mice were fragile, with reduced type X collagen expression, disturbed collagen fibril arrangement, increased chondrocyte apoptosis and premature matrix mineralization. Furthermore, a physiological concentration of leptin altered type X collagen mRNA expression, cell cycle, apoptosis and calcification during ATDC5 chondrocytic cell culture and primary chondrocyte differentiation culture in vitro. These findings suggest that a physiological level of leptin plays an essential role in the regulation of chondrocyte differentiation and cartilage matrix maturation in the growth plate, via a peripheral endocrine or paracrine mechanism, which may in turn alter the rate of longitudinal bone growth. However, further investigation is needed to clarify the role of peripheral leptin in endochondral ossification, regulation mechanisms and clinical implications.

Acknowledgments

We thank Ms. Kanae Asai, Ms. Mina Okamoto, Mr. Azusa Seki and Mr. Tsuyoshi Ishii for their excellent technical assistance, Dr. Shigeki Kakunaga for reviewing the manuscript and Dr. Takashi Sakai for providing invaluable advice. This work was supported by grants from the Ministry of Education, Culture, Sports, Science and Technology, Japan and the Osaka Medical Research Foundation for Incurable Disease.

References

[1] Zhang Y, Proenca R, Maffei M, Barone M, Leopold L, Friedman JM. Positional cloning of the mouse obese gene and its human homologue. Nature 1994;372:425–32.
[2] Campfield LA, Smith FJ, Guisez Y, Devos R, Burn P. Recombinant mouse OB protein: evidence for a peripheral signal linking adiposity and central neural networks. Science 1995;269:546–9.
[3] Hoggard N, Hunter L, Duncan JS, Williams LM, Trayhurn P, Mercer JG. Leptin and leptin receptor mRNA and protein expression in the murine fetus and placenta. Proc Natl Acad Sci U S A 1997;94:11073–8.
[4] Wang J, Liu R, Hawkins M, Barzilai N, Rossetti L. A nutrient-sensing pathway regulates leptin gene expression in muscle and fat. Nature 1998;393:684–8.
[5] Castellucci M, De Matteis R, Meisser A, Cancello R, Monsurro V, Islami D, et al. Leptin modulates extracellular matrix molecules and metalloproteinases: possible implications for trophoblast invasion. Mol Hum Reprod 2000;6:951–8.
[6] Reseland JE, Syversen U, Bakke I, Qvigstad G, Eide LG, Hjertner O, et al. Leptin is expressed in and secreted from primary cultures of human osteoblasts and promotes bone mineralization. J Bone Miner Res 2001;16:1426–33.
[7] Tartaglia LA, Dembski M, Weng X, Deng N, Culpepper J, Devos R, et al. Identification and expression cloning of a leptin receptor. OB-R Cell 1995;83:1263–71.
[8] Steppan CM, Crawford DT, Chidsey-Frink KL, Ke H, Swick AG. Leptin is a potent stimulator of bone growth in ob/ob mice. Regul Pept 2000;92:73–8.
[9] Kume K, Satomura K, Nishisho S, Kitaoka E, Yamanouchi K, Tobiume S, et al. Potential role of leptin in endochondral ossification. J Histochem Cytochem 2002;50:159–69.
[10] Montague CT, Farooqi IS, Whitehead JP, Soos MA, Rau H, Wareham NJ, et al. Congenital leptin deficiency is associated with severe early-onset obesity in humans. Nature 1997;387:903–8.
[11] Ozata M, Ozdemir IC, Licinio J. Human leptin deficiency caused by a missense mutation: multiple endocrine defects, decreased sympathetic tone, and immune system dysfunction indicate new targets for leptin action, greater central than peripheral resistance to the effects of leptin, and spontaneous correction of leptin-mediated defects. J Clin Endocrinol Metab 1999;84:3686–95.
[12] Charlton HM. Mouse mutants as models in endocrine research. Q J Exp Physiol 1984;69:655–76.
[13] Farooqi IS, Jebb SA, Langmack G, Lawrence E, Cheetham CH, Prentice AM, et al. Effects of recombinant leptin therapy in a child with congenital leptin deficiency. N Engl J Med 1999;341:879–84.
[14] Lee K, Lanske B, Karaplis AC, Deeds JD, Kohno H, Nissenson RA, et al. Parathyroid hormone-related peptide delays terminal differentiation of chondrocytes during endochondral bone development. Endocrinology 1996;137:5109–18.
[15] Vu TH, Shipley JM, Bergers G, Berger JE, Helms JA, Hanahan D, et al. MMP-9/gelatinase B is a key regulator of growth plate angiogenesis and apoptosis of hypertrophic chondrocytes. Cell 1998;93:411–22.
[16] Alvarez J, Horton J, Sohn P, Serra R. The perichondrium plays an important role in mediating the effects of TGF-beta1 on endochondral bone formation. Dev Dyn 2001;221:311–21.
[17] Maes C, Carmeliet P, Moermans K, Stockmans I, Smets N, Collen D, et al. Impaired angiogenesis and endochondral bone formation in mice lacking the vascular endothelial growth factor isoforms VEGF164 and VEGF188. Mech Dev 2002;111:61–73.
[18] Namae M, Mori Y, Yasuda K, Kadowaki T, Kanazawa Y, Komeda K. New method for genotyping the mouse Lep(ob) mutation, using a polymerase chain reaction assay. Lab Anim Sci 1998;48:103–4.
[19] Hoggard N, Mercer JG, Rayner DV, Moar K, Trayhurn P, Williams LM. Localization of leptin receptor mRNA splice variants in murine

peripheral tissues by RT-PCR and in situ hybridization. Biochem Biophys Res Commun 1997;232:383–7.
[20] Brighton CT. The growth plate. Orthop Clin North Am 1984; 15:571–95.
[21] Pavlov MI, Sautier JM, Oboeuf M, Asselin A, Berdal A. Chondrogenic differentiation during midfacial development in the mouse: in vivo and in vitro studies. Biol Cell 2003;95:75–86.
[22] Ratisoontorn C, Seto ML, Broughton KM. Cunningham, In vitro differentiation profile of osteoblasts derived from patients with Saethre–Chotzen syndrome. Bone 2005;36:627–34.
[23] Atsumi T, Miwa Y, Kimata K, Ikawa Y. A chondrogenic cell line derived from a differentiating culture of AT805 teratocarcinoma cells. Cell Differ Dev 1990;30:109–16.
[24] Shukunami C, Shigeno C, Atsumi T, Ishizeki K, Suzuki F, Hiraki Y. Chondrogenic differentiation of clonal mouse embryonic cell line ATDC5 in vitro: differentiation-dependent gene expression of parathyroid hormone (PTH)/PTH-related peptide receptor. J Bone Miner Res 1996;133:457–68.
[25] Shukunami C, Ishizeki K, Atsumi T, Ohta Y, Suzuki F, Hiraki Y. Cellular hypertrophy and calcification of embryonal carcinoma-derived chondrogenic cell line ATDC5 in vitro. J Bone Miner Res 1997;12:1174–88.
[26] Wauters M, Considine R, Lofgren A, Van Broeckhoven C, Van der Auwera JC, De Leeuw I, et al. Associations of leptin with body fat distribution and metabolic parameters in non-insulin-dependent diabetic patients: no effect of apolipoprotein E polymorphism. Metabolism 2000;49:724–30.
[27] Haluzik M, Fiedler J, Nedvidkova J, Ceska R. Serum leptin levels in patients with hyperlipidemias. Nutrition 2000;16:429–33.
[28] Maor G, Rochwerger M, Segev Y, Phillip M. Leptin acts as a growth factor on the chondrocytes of skeletal growth centers. J Bone Miner Res 2002;17:1034–43.
[29] Ducy P, Amling M, Takeda S, Priemel M, Schilling AF, Beil FT, et al. Leptin inhibits bone formation through a hypothalamic relay: a central control of bone mass. Cell 2000;100:197–207.
[30] Takeda S, Elefteriou F, Levasseur R, Liu X, Zhao L, Parker KL, et al. Leptin regulates bone formation via the sympathetic nervous system. Cell 2002;111:305–17.
[31] Dal Farra C, Zsurger N, Vincent JP, Cupo A. Binding of a pure 125I-monoiodoleptin analog to mouse tissues: a developmental study. Peptides 2000;21:577–87.
[32] Figenschau Y, Knutsen G, Shahazeydi S, Johansen O, Sveinbjornsson B. Human articular chondrocytes express functional leptin receptors. Biochem Biophys Res Commun 2001;287:190–7.
[33] Shimon I, Yan X, Magoffin DA, Friedman TC, Melmed S. Intact leptin receptor is selectively expressed in human fetal pituitary and pituitary adenomas and signals human fetal pituitary growth hormone secretion. J Clin Endocrinol Metab 1998;83:4059–64.
[34] Jacenko O, LuValle PA, Olsen BR. Spondylometaphyseal dysplasia in mice carrying a dominant negative mutation in a matrix protein specific for cartilage-to-bone transition. Nature 1993;365: 56–61.
[35] Gibson G, Lin DL, Francki K, Caterson B, Foster B. Type X collagen is colocalized with a proteoglycan epitope to form distinct morphological structures in bovine growth cartilage. Bone 1996;19: 307–315.
[36] Loder RT. The demographics of slipped capital femoral epiphysis. An international multicenter study. Clin Orthop 1996;322:8–27.
[37] Hassink SG, Sheslow DV, de Lancey E, Opentanova I, Considine RV, Caro JF. Serum leptin in children with obesity: relationship to gender and development. Pediatrics 1996;98:201–3.
[38] Gordeladze JO, Drevon CA, Syversen U, Reseland JE. Leptin stimulates human osteoblastic cell proliferation, de novo collagen synthesis, and mineralization: impact on differentiation markers, apoptosis, and osteoclastic signaling. J Cell Biochem 2002;85: 825–836.
[39] Elefteriou F, Ahn JD, Takeda S, Starbuck M, Yang X, Liu X, et al. Leptin regulation of bone resorption by the sympathetic nervous system and CART. Nature 2005;434:514–20.
[40] Hamrick MW, Pennington C, Newton D, Xie D, Isales C. Leptin deficiency produces contrasting phenotypes in bones of the limb and spine. Bone 2004;34:376–83.
[41] Luo G, Ducy P, McKee MD, Pinero GJ, Loyer E, Behringer RR, et al. Spontaneous calcification of arteries and cartilage in mice lacking matrix GLA protein. Nature 1997;386:78–81.
[42] Schwartz Z, Soskolne WA, Neubauer T, Goldstein M, Adi S, Ornoy A. Direct and sex-specific enhancement of bone formation and calcification by sex steroids in fetal mice long bone in vitro biochemical and morphometric study. Endocrinology 1991;129:1167–74.
[43] Nilsson A, Ohlsson C, Isaksson OG, Lindahl A, Isgaard J. Hormonal regulation of longitudinal bone growth. Eur J Clin Nutr 1994;48(Suppl 1):S150–8.

ARTHRITIS & RHEUMATISM
Vol. 52, No. 8, August 2005, pp 2559–2566
DOI 10.1002/art.21154

Microbubble-Enhanced Ultrasound Exposure Promotes Uptake of Methotrexate Into Synovial Cells and Enhanced Antiinflammatory Effects in the Knees of Rabbits With Antigen-Induced Arthritis

Hiroyuki Nakaya,[1] Tominaga Shimizu,[2] Ken-ichi Isobe,[2] Keiji Tensho,[2] Takahiro Okabe,[2] Yukio Nakamura,[2] Masashi Nawata,[2] Hideki Yoshikawa,[1] Kunio Takaoka,[3] and Shigeyuki Wakitani[2]

Objective. **To evaluate whether microbubble-enhanced ultrasound (US) treatment promotes the delivery of methotrexate (MTX) into synovial cells and the enhanced antiinflammatory effects of intraarticular MTX therapy in a rabbit arthritis model.**

Methods. **Arthritis was induced in both knees of 53 rabbits by immunization with ovalbumin. MTX including a microbubble agent was then injected into the left and right knee joints, and the right knees were exposed to US (MTX+/US+ group), while the left knees were not (MTX+/US− group). The knee joints were evaluated histologically in 7 rabbits at 5 time points up to day 56. Quantitative gene expression of interleukin-1β (IL-1β) in synovial tissue was measured on days 7 and 28. Eight rabbits were used for the measurement of MTX concentration in synovial tissue 12 hours after treatment. To evaluate the effect of microbubble-enhanced US treatment in the absence of MTX, only the microbubble agent was injected into the left and right knee joints of 10 rabbits with or without US exposure, and these animals were evaluated histologically on days 7 and 28.**

Results. **The MTX concentration in synovial tissue was significantly higher in the MTX+/US+ group than in the MTX+/US− group. Synovial inflammation was less prominent in the MTX+/US+ group compared with the MTX+/US− group, judging from the results of the histologic evaluation and the gene expression levels of IL-1β in synovial tissue. It also appeared that microbubble-enhanced US exposure itself did not affect inflammation.**

Conclusion. **Microbubble-enhanced US exposure promoted the uptake of MTX into synovial cells, which resulted in enhancement of the antiinflammatory effects of the intraarticular MTX injection. These results suggest that application of this technique may have clinical benefit.**

Rheumatoid arthritis (RA) is a systemic inflammatory disorder characterized by pain, swelling, and destruction of the affected joints. The exact mechanism of RA pathogenesis is not well understood. Recently, remarkable progress in the area of anticytokine therapy has provided an alternative and successful approach for therapeutic intervention in RA. However, methotrexate (MTX) still plays a central role in the treatment of RA, although administration of this agent sometimes causes serious side effects, such as interstitial pneumonia, renal failure, and myelosuppression. Intraarticular injection of MTX is thought to be safe compared with the systemic administration of this agent, although the clinical effectiveness in controlling synovitis in RA patients is controversial. Most studies have documented insufficient antiinflammatory effects (1–3). Mechanisms of resis-

Supported in part by the Japanese Ministry of Education, Culture, Sports, Science and Technology (grants 15591572 and 16390436).

[1]Hiroyuki Nakaya, MD, Hideki Yoshikawa, MD, PhD: Osaka University Medical School, Suita, Japan; [2]Tominaga Shimizu, MD, PhD, Ken-ichi Isobe, MD, Keiji Tensho, MD, Takahiro Okabe, MD, Yukio Nakamura, MD, Masashi Nawata, MD, Shigeyuki Wakitani, MD, PhD: Shinshu University School of Medicine, Matsumoto, Japan; [3]Kunio Takaoka, MD, PhD: Osaka City University Medical School, Osaka, Japan.

Address correspondence and reprint requests to Shigeyuki Wakitani, MD, PhD, Shinshu University School of Medicine, Asahi 3-1-1, Matsumoto 390-8621, Japan. E-mail: wakitani@hsp.md.shinshu-u.ac.jp.

Submitted for publication January 5, 2005; accepted in revised form April 14, 2005.

tance to MTX are considered to consist of 3 parts: decreased transport, impaired polyglutamylation, and increased dihydrofolate reductase enzyme activity (4–6). It has been reported that there is a significant correlation between reduced levels of folate carrier protein (one of the MTX transporters) at diagnosis and the histologic responses to preoperative MTX chemotherapy for osteosarcoma (6). From these observations, it is possible to conclude that the efficacy of MTX is limited by its transport into cells. Thus, we hypothesized that poor delivery of MTX into RA synovial cells would lead to poor clinical efficacy of intraarticular MTX injection therapy.

To facilitate uptake of MTX into synovial cells, we chose an ultrasound (US) treatment technique (sonoporation) with enhancement by the use of an echo-contrast microbubble agent. Previous reports have indicated that US exposure increases transfection efficiency of gene constructs, due to increased cell membrane porosity and acoustic cavitation (7,8), which is enhanced with the use of microbubble agents. This is one of the best techniques for in vivo work and clinical applications because it is simple and noninvasive. Additionally, there are no viral components, although the success rate for induction is lower than that found with viral technologies in vitro and in vivo, as previously reported (9–12). Our findings in the present study indicate that US irradiation treatment with a microbubble agent enhances the antiinflammatory effect of intraarticular MTX injection in an ovalbumin (OVA)–induced arthritis model in rabbits.

MATERIALS AND METHODS

In vitro induction of fluorescence-conjugated MTX. As an initial step, we determined the optimum concentration of echo-contrast microbubbles (Optison; Mallinckrodt, St. Louis, MO) for MTX (Iatron, Tokyo, Japan) induction into synovial cells. In vitro induction was performed according to a previously described procedure (10). Synovial cells were obtained during total knee arthroplasty from 2 RA patients, who had provided informed consent. Briefly, the tissue was minced and incubated with 0.25% collagenase (Roche, Indianapolis, IN) in phosphate buffered saline (PBS) for 2 hours at 37°C under continuous agitation. The cells were collected by centrifugation, resuspended, and cultured in Dulbecco's modified Eagle's medium (Invitrogen, Carlsbad, CA) containing 10% fetal calf serum and antibiotics (100 units/ml penicillin, 0.1 mg/ml streptomycin, 0.25 μg/ml amphotericin B; Invitrogen). Cultured cells were trypsinized, washed twice in PBS, and resuspended at 1×10^5/ml of PBS per well in a 48-well plate. Optison was added to the cell medium at concentrations of 0%, 5%, 10%, and 20%. Then, 10 μg of Texas Red–conjugated MTX (Molecular Probes, Leiden, The Netherlands) was added to the cell supernatant in each well.

The US probe and well plate were firmly fixed to a stand to avoid dislocation during US exposure. Immediately after fluorescent MTX and microbubbles were added to the well, US exposure was performed. The sonoporator (Sonitron 2000; Mallinckrodt) settings were as follows: frequency 1 MHz, duration 30 seconds, power 1.0 W/cm^2, duty cycle 10%, and probe diameter 0.5 cm. The US probe was inserted directly into the cell suspension. A miniature stirrer was placed within the well and spun at 300 revolutions per minute to prevent cell adhesion to the plate. The cells were placed a row apart from each other to prevent interaction due to the transmission of US between the wells. After US exposure, cell viability was tested by counting the cells stained with trypan blue. The cell suspensions were harvested from the wells and attached to slides using a Cyto-Tek centrifuge (Sakura, Tokyo, Japan) at 1,500 rpm for 5 minutes. Texas Red–positive cells were detected by fluorescence microscopy. The average induction efficiency was calculated as the ratio of incorporated cells to all cells in 5 fields.

In vivo induction of fluorescence-conjugated MTX. To confirm that MTX induction into synovial in vivo cells would be promoted by microbubble-enhanced US treatment, we designed in vivo experiments. Three NZW rabbits (Japan SLC, Hamamatsu, Japan) weighing 2.5, 2.7, and 2.8 kg were anesthetized by intramuscular injection of a mixture of ketamine (100 mg/ml [0.6 ml/kg body weight]; Sankyo, Tokyo, Japan) and xylazine (20 mg/ml [0.3 ml/kg body weight]; Bayer, Leverkusen, Germany). We injected 50 μg of Texas Red–conjugated MTX with 5% Optison in 2.5 ml saline, making sure to diffuse it into the left and right knee joints. Soon after injection, US exposure was applied in the medial, central, and lateral areas of the suprapatellar pouch of the right knees for 2 minutes per application. US treatment was not performed in the left knees. US was administered with a sonoporator using the following settings: frequency 1 MHz, duration 2 minutes, power 2.0 W/cm^2, duty cycle 50%, and probe diameter 3 cm. Then, the rabbits were killed by excessive intravenous injection of anesthetic agents. Synovial tissue, with the associated muscle and tendon of the suprapatellar pouch of the joints, was obtained and dissected sagittally at the center. It was immediately chilled in liquid nitrogen. Sections of 7-μm thickness were cut in a cryostat, air-dried on slides, fixed in 4% paraformaldehyde, and stained with hematoxylin for counterstaining. The sections were examined by fluorescence microscopy.

Antigen-induced arthritis (AIA) in the rabbit knee. Sixty-two NZW rabbits, each weighing ~2.7 kg (2.5–3.1 kg) were anesthetized as described above. They then received intradermal injections of 4 mg OVA (Sigma, St. Louis, MO) in 0.5 ml Freund's complete adjuvant (Difco, Detroit, MI) and 0.5 ml PBS 3 times at 7-day intervals, as previously reported (13). Five days after the third injection, 1.5 mg OVA in 0.5 ml sterile saline was injected into the left and right knee joints of the rabbits. After confirming the establishment of arthritis 10 days after the injection, the experimental procedures were started. Fifty-three of the 62 rabbits (85%) showed signs of arthritis in both knees and were used for the experiments. In preliminary experiments, we confirmed that the inflammation was virtually identical histologically in both knees (data not shown).

MTX injection and US treatment. We injected 0.1% MTX with 5% Optison (from the initial in vitro experiment described above) in 2.5 ml saline, ensuring diffusion into both knee joints of 43 rabbits that were anesthetized as described above. US was administered to the right knee in the same manner (MTX+/US+ group). US treatment was not performed on the left knees (MTX+/US− group). Seven rabbits each were killed on days 3, 7, 14, 28, and 56 for histologic examination. The remaining 8 rabbits were used for measurement of MTX in synovial tissue.

To determine whether microbubble-enhanced US itself affected inflammation of synovial tissue, we injected 5% Optison without MTX in 2.5 ml saline into the left and right knee joints of the other 10 rabbits. Then, US was administered to the right knees (MTX−/US+ group) in the same manner as described above, while the left knees were not exposed (MTX−/US− group). Five rabbits each were killed on days 7 and 28 for histologic evaluation.

Histologic evaluation. Synovial tissue from the suprapatellar pouch of the joints was obtained at each time point. It was dissected sagittally at the center, washed, and fixed in 10% formaldehyde in PBS. It was then rinsed with deionized water and dehydrated in a graded ethanol series. Dehydrated tissue was embedded in paraffin, cut into 5-μm sections, mounted on glass slides precoated with poly-L-lysine, dried overnight at 50°C, and stained with hematoxylin and eosin (H&E).

Distal femurs were cut sagittally in the center of the patellar groove and fixed in 10% formaldehyde, decalcified in 10% EDTA, embedded in paraffin, cut into 5-μm sections, and stained with H&E and toluidine blue.

To evaluate the degree of synovial inflammation, we used modified scoring criteria as previously described by Sanchez-Pernaute and colleagues (14). These criteria (Table 1) consist of 5 categories: inflammatory cell infiltration, synovial lining layers, villus formation, vascularity, and cartilage damage. Synovial tissue was scored depending on the degree of inflammation (from 0 for normal tissue to 18 for most severe inflammation). Sections were examined blindly and scored independently by 3 of the authors (KT, TO, YN), without knowledge of the group being examined.

Immunohistochemistry. To identify blood vessels accurately, anti-α-smooth muscle actin (α-SMA) immunostaining was performed using the mouse monoclonal anti-α-SMA antibody (1A4; Dako, Carpinteria, CA) and the Envision Plus HRP system (K4006; Dako). Formalin-fixed paraffinized sections of rabbit synovial tissue were baked, dewaxed, and rehydrated prior to a peroxidase block (0.1% [volume/volume] H_2O_2). The primary antibody and the horseradish peroxide–labeled polymer were used as per the Dako Envision kit, followed by staining with 3,3′-diaminobenzidine and counterstaining with hematoxylin before mounting. A negative control was prepared by omitting the primary antibody. A positive control was prepared on the vessels of the same section.

Measurement of MTX concentrations. MTX and Optison in 2.5 ml saline were injected into the left and right knee joints of 8 rabbits. US was administered to the right knees in the same manner, while the left knees were not exposed to US. The concentration of MTX in the synovial tissue of 8 rabbits was measured by the enzyme immunoassay method with an MTX assay kit (Iatron) 12 hours after US irradiation. Briefly, the synovial tissue excised from the surface of inflamed synovium was homogenized in Tris buffer (pH 7.4; 3 ml/gm tissue), boiled for 5 minutes, and then centrifuged at 30,000 rpm for 30 minutes in a 4°C atmosphere. This was followed by the addition of 0.1 ml of the supernatant in 1 ml of reagent composed of dihydrofolate reductase (enzyme), NADPH (coenzyme), and 0.1 ml of dihydrofolate (substrate). The residual activity of the dihydrofolate reductase was assayed by absorptiometry at a wavelength of 340 nm.

Table 1. Scoring system for histologic evaluation

Parameter	Scoring
Inflammation	0 = normal 1 = minimal inflammatory infiltration 2 = mild inflammatory infiltration 3 = moderate inflammatory infiltration 4 = marked infiltration with marked edema 5 = severe infiltration with edema
Synovial lining layers	0 = normal (1–2 cell layers) 1 = slightly hyperplasia (2–3 cell layers) 2 = moderate (3–5 cell layers) 3 = pronounced (5 or more cell layers)
Villus formation	0 = none 1 = minimal (1–2 villi) 2 = several (3 or more villi)
Vascularity	0 = normal (limited number of blood vessels) 1 = slightly hypervascular (focal occurrence of a small number of blood vessels) 2 = moderate (focal occurrence of a large number of blood vessels) 3 = pronounced (broadly distributed and large number of blood vessels)
Cartilage damage	0 = normal 1 = minimal (loss of toluidine blue staining only) 2 = mild (loss of toluidine blue staining and mild cartilage thinning) 3 = moderate (moderate diffuse or multifocal cartilage loss) 4 = marked (marked diffuse or multifocal cartilage loss) 5 = severe (diffuse or multifocal cartilage loss)

Real-time polymerase chain reaction (PCR). Synovial tissue was obtained and messenger RNA (mRNA) expression was assessed quantitatively in 7- and 28-day samples of the MTX+/US+ and MTX+/US− groups. PCR primers and fluorogenic probes of interleukin-1β (IL-1β) (forward 5′-TTGCTGAGCCAGCCTCTCTT-3′, reverse 5′-GCTGGGTACCAAGGTTCTTTGA-3′, TaqMan 5′-TGCCATTCAGGCAAGGCCAGC-3′) were designed according to the published sequences (GenBank accession no. M_26295) using Primer Express software (Perkin-Elmer Applied Biosystems, Foster City, CA). They were obtained purified by high-performance liquid chromatography from Applied Biosystems. The fluorogenic probes contained a reporter dye (FAM) covalently linked at the 5′ end and a quencher dye (TAMRA) covalently attached at the 3′ end. Extension from the 3′ end was blocked by the attachment of a 3′-phosphate group.

As external controls for the target gene, plasmid recombinants containing the specific target sequence were

generated, as well as 18S ribosomal RNA (rRNA; Perkin-Elmer Applied Biosystems). For this purpose, total RNA from individuals positive for the allele of interest was extracted and reverse transcribed as described above. Following reverse transcription and allele-specific PCR, amplicons were cloned using pCR 2.1 TOPO (Invitrogen). Recombinant plasmids were expressed in competent *Escherichia coli* (INVαF'; Invitrogen). Plasmid DNA was isolated using silica cartridges (QIAprep Spin Miniprep Kit; Qiagen, Hilden, Germany). Sequences of the cloned amplicons were verified using an automated sequencer (ABI PRISM 7700; Perkin-Elmer Applied Biosystems) with universal M13 primers. Concentrations of the recombinant plasmids were determined by optical density spectrometry. Serial dilutions from the resulting clones were used for standardization, as described in detail in the manufacturer's bulletin.

PCR was performed using 300 n*M* forward and reverse primers and 200 n*M* TaqMan probe (final concentration). Each PCR amplification was performed in triplicate wells using the following temperature and cycling profile: 50°C for 2 minutes and 95°C for 10 minutes, followed by 40 cycles of 95°C for 15 seconds and 58°C for 1 minute (15).

The relative expression of IL-1β alleles was determined with reference to the total amount of IL-1β mRNA after normalization against 18S rRNA as implemented in the ABI PRISM 7700 Sequence Detection System software. Results were considered only if the analysis of IL-1β showed all reactions to have the same amount of amplification as 18S rRNA. This procedure allowed for comparison of group-specific IL-1β expression as well as the total expression levels of 18S rRNA.

Statistical analysis. Results are expressed as the mean ± SD. The significance of the difference in histologic scores between the MTX+/US+ and MTX+/US− groups at the various posttreatment times (days 3, 7, 14, 28, and 56) was tested using two-way factorial analysis of variance (ANOVA), followed by Student's paired *t*-test for comparison.

The difference in histologic scores among the MTX+/US+ group and the other 3 control groups (MTX+/US−, MTX−/US+, and MTX−/US−) at 7 and 28 days was compared by Student's paired *t*-test. Student's paired *t*-test was also used to analyze the results of MTX concentration and real-time reverse transcriptase–PCR. *P* values less than 0.05 were considered significant.

RESULTS

In vitro MTX induction into synovial cells. To confirm the promotion of MTX induction into RA synovial cells by US irradiation and to determine the optimum concentration of Optison, fluorescence-conjugated MTX was administered into RA synovial cells by sonoporation in vitro. In the absence of US, MTX was administered into a few synovial cells. With US exposure, the administration rate was increased to almost 5% for MTX alone, and ~31% with 5% Optison (Figure 1). Further increases in the concentration of this reagent elevated the induction rate to a maximum of 48%. For the studies described here, 5% Optison was used in each of the experiments.

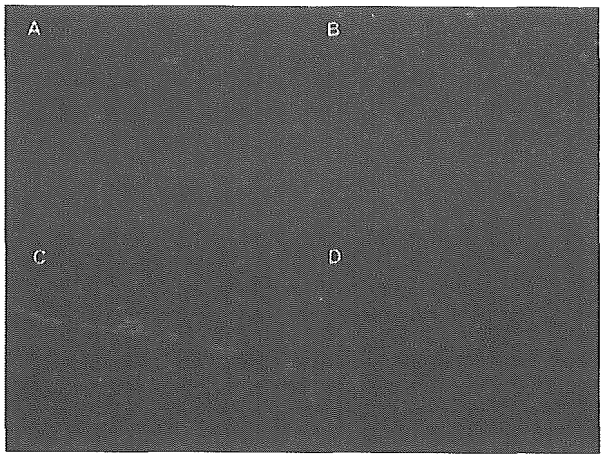

Figure 1. Fluorescence photomicrographs of synovial cells and tissue treated with Texas Red–conjugated methotrexate (MTX). Texas Red–conjugated MTX was administered to rheumatoid arthritis (RA) synovial cells by sonoporation in vitro alone (**A**) or with 5% Optison (**B**). Synovial tissue was collected from joints after injection of Texas Red–conjugated MTX with 5% Optison, with (**C**) or without (**D**) ultrasound (US) treatment. The upper parts of **C** and **D** show the joint cavity. Without Optison, almost 5% of cells were fluorescence positive (**A**). The ratio of fluorescence-positive cells was elevated to ~31% with the addition of 5% Optison (**B**). In several layers of the synovial lining, with US treatment, fluorescence-positive cells were observed (**C**). Without US, only a weakly positive area was observed (**D**). (Original magnification × 200.)

In vivo MTX induction into synovial cells. To confirm the promotion of MTX induction in vivo into RA synovial cells by US treatment, fluorescence-conjugated MTX was administered into RA synovial cells by sonoporation in vivo. In the presence of US, fluorescence-positive cells were observed in several synovial lining layers, while only a weakly positive area was observed in the absence of US (Figure 1). The Texas Red–positive area was restricted to synovial cells, and was not observed in other tissue such as tendon or muscle in either group.

MTX concentration. The MTX concentrations in synovial tissue were measured in the MTX+/US+ and MTX+/US− groups (8 samples each) 12 hours after the injection of MTX and Optison. The mean ± SD weight of the tissue from right knees (the MTX+/US+ group) was 454 ± 37.0 mg, while that from left knees (the MTX+/US− group) was 467 ± 44.4 mg. There was no significant difference between these groups. The mean ± SD MTX concentration in the MTX+/US+ group was estimated at $7.575 \pm 1.590 \times 10^{-7}$ mg/dl,

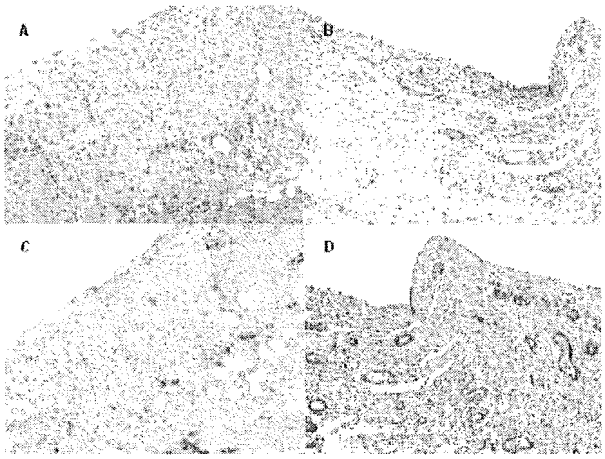

Figure 2. Day-7 histologic images of synovial tissue in the MTX+/US+ group and the MTX+/US− group. **A** and **B,** Hematoxylin and eosin staining. **C** and **D,** Immunohistochemical staining with anti–α-smooth muscle actin antibody. **A** and **C,** In the MTX+/US+ group (histologic score 3), minimal inflammatory cell infiltration, several synovial lining layers, no villus formation, and slight hypervascularity were observed. **B** and **D,** In the MTX+/US− group (histologic score 9), marked inflammatory cell infiltration, proliferating synovial lining layers (as many as 5 layers), no villus formation, and general occurrence of a large number of blood vessels were seen. See Figure 1 for definitions. (Original magnification × 40.)

while that in the MTX+/US− group was 2.875 ± 0.7889×10^{-7} mg/dl ($P < 0.01$).

Histologic findings. In the MTX+/US+ group, moderate inflammation (inflammatory cell infiltration, thickened synovial lining layers, and hypervascularity) was observed after 3 days, but it became less severe over a period from 7 to 56 days. Evidence of inflammation decreased in the synovial lining layer and the vascular network. In the MTX+/US− group, moderate inflammation similar to that seen in the MTX+/US+ group was observed after 3 days, continued until 28 days, and became less severe after 56 days.

After 7 days (Figure 2), in the MTX+/US+ group, minimal inflammatory cell infiltration and slight hypervascularity (minimal inflammation) were observed. In the MTX+/US− group, marked inflammatory cell infiltration, proliferating synovial lining layers (as many as 5), and proliferating blood vessels (moderate inflammation) were observed.

After 28 days (Figure 3), in the MTX+/US+ group, moderately proliferating synovial lining layers and focal proliferation of a small number of blood vessels (minimal inflammation) were observed. In the MTX+/US− group, marked inflammatory cell infiltration, proliferating synovial lining layers (>5 cell layers), and general proliferation of blood vessels (moderate inflammation) were observed.

After 56 days, both groups showed moderately proliferating synovial lining layers and focal proliferation of a small number of blood vessels (minimal inflammation). There was no significant difference between the 2 groups.

Articular cartilage was examined histologically for signs of damage caused by US exposure and/or MTX injection. A very slight decrease in the intensity of metachromatic staining (histologic scoring 0 or 1) in the surface area was observed in some samples of the MTX+/US+ and MTX+/US− groups on days 7 and 28.

Histologic scores. The mean ± SD histologic scores at 3, 7, 14, 28, and 56 days after treatment were 9.00 ± 0.31, 5.42 ± 0.30, 4.71 ± 0.18, 4.57 ± 0.37, and 5.57 ± 0.30, respectively, in the MTX+/US+ group, and 8.42 ± 0.20, 8.57 ± 0.37, 8.43 ± 0.20, 8.29 ± 0.36, and 5.71 ± 0.29 in the MTX+/US− group. The scores in the MTX+/US+ group and the MTX+/US− group were significantly different by two-way factorial ANOVA ($P < 0.05$). In addition, when we compared them at each

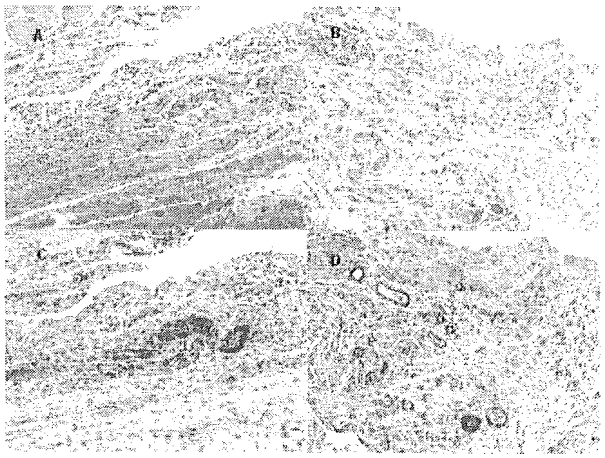

Figure 3. Day-28 histologic images of synovial tissue in the MTX+/US+ group and the MTX+/US− group. **A** and **B,** Hematoxylin and eosin staining. **C** and **D,** Immunohistochemical staining with anti–α-smooth muscle actin antibody. **A** and **C,** In the MTX+/US+ group (histologic score 5), minimal inflammatory cell infiltration, a moderate number of synovial lining layers, no villus formation, and focal occurrence of a small number of blood vessels were seen. **B** and **D,** In the MTX+/US− group (histologic score 10), marked inflammatory cell infiltration with marked edema, >5 pronounced synovial lining layers, no villus formation, and a broadly distributed large number of blood vessels were seen. See Figure 1 for definitions. (Original magnification × 40.)

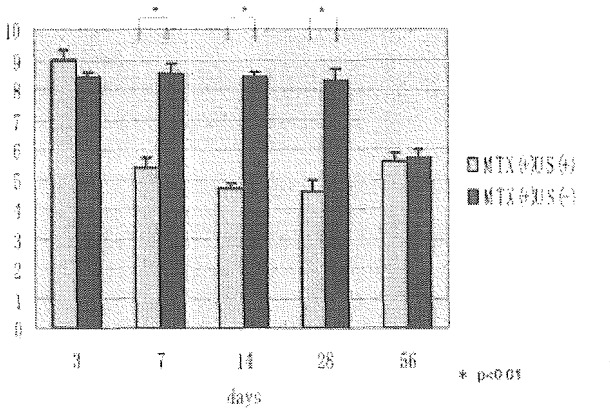

Figure 4. Histologic scores of synovial tissue from patients in the MTX+/US+ and MTX+/US− groups at each time point. Values are the mean and SD. *P* values were determined using two-way factorial analysis of variance. See Figure 1 for definitions.

time point using Student's paired *t*-test, the scores in the MTX+/US+ group at 7, 14, and 28 days were significantly better than those in the MTX+/US− group (Figure 4).

To confirm that the antiinflammatory effect was not due to US exposure, we injected the right knees with Optison only and exposed them to US (MTX−/US+ group). Scores in the MTX+/US+, MTX+/US−, MTX−/US+, and MTX−/US− groups were compared on days 7 and 28, and a significant difference was

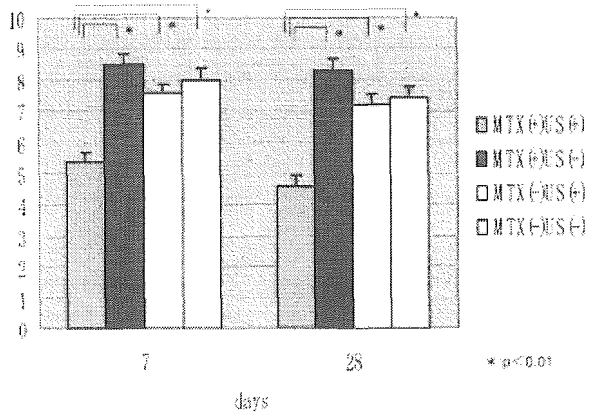

Figure 5. Histologic scores of synovial tissue from patients in the MTX+/US+, MTX+/US−, MTX−/US+, and MTX−/US− groups 7 and 28 days after treatment. Values are the mean and SD. See Figure 1 for definitions.

observed between the MTX+/US+ group and the other 3 groups ($P < 0.05$) (Figure 5).

Findings of real-time PCR. Using real-time PCR, we examined the quantitative gene expression of IL-1β in synovial tissue obtained 7 and 28 days after US irradiation. The mean ± SD expression 7 and 28 days after treatment was 1.3×10^{-3} (1.5×10^{-4}) and 3.3×10^{-3} (2.5×10^{-4}), respectively, in the MTX+/US+ group, and 8.6×10^{-2} (9.0×10^{-3}) and 8.4×10^{-2} (1.2×10^{-3}) in the MTX+/US− group. There was a significant difference ($P < 0.01$) between the groups at each time point.

DISCUSSION

Our results show that, in a rabbit arthritis model, microbubble-enhanced US treatment promotes uptake of MTX into synovial cells, which results in acceleration of antiinflammatory effects following intraarticular MTX injection. The antiinflammatory effect was confirmed by histologic scoring and expression of IL-1β mRNA in synovial tissue. The increased uptake of MTX into synovial cells was confirmed histologically by analysis of MTX concentration in synovial tissue and induction of Texas Red–conjugated MTX in vitro and in vivo. To confirm that the antiinflammatory effect was not due to US irradiation treatment with or without Optison, we injected Optison only (without MTX), and administered US to the right knees in the rabbits. Because there was no antiinflammatory effect, we concluded that neither microbubble injection with US exposure nor MTX injection has an antiinflammatory effect. However, the combination of MTX, microbubble injection, and US exposure was very effective. To our knowledge, this is the first report to describe the use of US in conjunction with antiinflammatory joint therapy in vivo. US gained attention through its use in gene therapy and tissue engineering. It is safe, minimally invasive, and can accommodate different therapeutic applications.

An antiinflammatory effect of this procedure (significantly reduced histologic inflammation and IL-1β gene expression in the synovial tissue) was observed from 7 to 28 days, but not at 56 days. All of the inflamed synovium of the joint cannot be covered by the use of a US probe applied at the skin surface. Indeed, histologic evaluation of inflammation of synovial tissue in the femorotibial joint, where US was not administered, revealed no difference from that in the control group (data not shown). Another explanation is that 56 days (exactly 66 days after immunization) may be enough to

decrease the inflammation of synovial tissue in AIA naturally.

One hypothesis regarding the mechanism for the efficacy of this procedure is that the bioeffects are consequences of inertial cavitation, violent oscillations, and the collapse of bubbles in the surrounding fluid. The Optison stock concentration is ~6.5×10^8/ml, and 5% Optison (3.25×10^7/ml) was injected into the joint. The microbubbles consist of hollow albumin filled with octafluoropropane. They are collapsed by the cavitation produced by US, and are considered to be eliminated quickly by distribution or phagocytosis. Physical and chemical phenomena related to inertial cavitation include microstreaming, shock waves, microjets, extremely high localized temperatures, pressures inside the bubbles, and generation of free radicals (16). If US causes promotion of induction through increased membrane porosity, as described above, it is reasonable to expect that there would be some limitations for transducible agents in terms of molecular size, 3-dimensional structure, and chemical compositions. In this study, we chose MTX (MW 454.45) as a transducive agent. Because we showed that Texas Red–conjugated MTX (MW 1,257.49) was also incorporated into cells in an in vitro experiment, molecules of this size should be readily incorporated into cells with this method. Uptake into cells of some genes or other pharmacologic agents that have an antiinflammatory effect can be promoted by microbubble-enhanced US exposure.

In vivo US and Optison conditions were selected based on in vitro data, and it is clear that there are significant differences between in vitro and in vivo conditions. Since the power of US is reduced by the long distance between the joint and the skin in vivo, it may be necessary to elevate the US power to a higher setting, provided there is no resultant heat production on the skin. In this study, output power (1–2W), duration (30 seconds to 2 minutes), and duty cycle (10–50%) were elevated.

Electroporation is also an effective MTX transduction technique. It has been widely used for transduction of genes and pharmacologic agents in vivo and in vitro. It does not require viral vector construction or virus preparation. Many reports describe electroporation as a technique for promoting electrochemotherapy through the uptake of MTX into cancer cells (17–19). We also showed that electrochemotherapy was effective in digital chondrosarcoma (20). However, the electrical fields created also affect normal tissue beyond the target site. Furthermore, cell anomalies or tissue damage after electroporation have often been observed. Thus, it is not an appropriate technique for the treatment of joints in RA patients. The encapsulation of MTX into cells with the use of a viral vector, recombinant polyomavirus–like particle, has been described (21), but this is a complex procedure and may not be suitable for clinical application.

MTX injection and US treatment can be used together in the clinic because of their low-risk safety profile. This technique may reduce synovitis in human arthritis and take the place of surgical synovectomy. It has been reported that surgical synovectomy of RA joints may offer short-term symptomatic relief but no retardation of the bone destruction or the disease process (22). While the benefits of our procedure might not match those of surgical excision of inflamed synovium, it is much less invasive than surgery and it can be performed frequently to obtain symptomatic relief. Further experiments are needed to determine whether this procedure alters the course of the disease. Furthermore, this technique can be applied in other inflammatory diseases.

For broader application in the clinic, there are some additional considerations that must be addressed. First, the intraarticular injection of MTX, which at high doses is sometimes used as an immunosuppressive agent, may cause adverse effects. The risk of iatrogenic infection warrants close attention. But MTX is reported to suppress production of superoxide and nitric oxide, and not to affect glycosaminoglycan synthesis of chondrocytes in vivo and in vitro (23,24).

Second, US may cause adverse effects. It has been reported that US increases matrix synthesis and that it does not affect the viability or proliferation of chondrocytes (25,26). The procedure reported here caused no harm to joint tissue apart from the proliferation zone in the synovium. However, the thick skin of the human joint may restrict the penetration of the ultrasonic vibration into synovial cells, which may cause a decrease in the uptake of MTX. The Sonitron is not approved for human use, but there is other equipment with greater power that is approved for human use in Japan (not for sonoporation). Longer exposure or higher power may cause local heat production. In such a case, a lower percentage setting of the duty cycle will help to prevent adverse effects. The optimal conditions necessary for the effective administration of US in humans need further investigation.

Third, the echo-contrast microbubbles may cause local or systemic side effects. These may include drug-induced allergic shock or joint pain because of high osmotic pressure. Moreover, another concern is that the overdosage of microbubbles or overexposure to ultra-